
Polarons: from single polaron to short scale phase separation.

V.V. Kabanov¹

J. Stefan Institute, Jamova 39, 1001, Ljubljana, Slovenia viktor.kabanov@ijs.si

1 Introduction

There is substantial evidence that the ground state in many of oxides is inhomogeneous[1]. In cuprates, for example neutron-scattering experiments suggest that phase segregation takes place in the form of stripes or short segments of stripes[2, 3]. There is some controversy whether this phase segregation is associated with magnetic interactions. On the other hand it is also generally accepted that the charge density in cuprates is not homogeneous.

The idea of charge segregation has a quite long history (see for example[4, 5, 6]). In charged systems the phase separation is often accompanied by the charge segregation. Breaking of the charge neutrality leads to the appearance of the electric field and substantial contribution of the electrostatic energy to the thermodynamic potential[7, 8]. Recently it was suggested that interplay of the short range lattice attraction and the long-range Coulomb repulsion between charge carriers could lead to the formation of short metallic [9, 10] or insulating[10, 11] stripes of polarons. If the attractive potential is isotropic, charged bubbles have a spherical shape. Kugel and Khomskii [12] suggested recently that the anisotropic attraction forces caused by Jahn-Teller centers could lead to the phase segregation in the form of stripes. The long-range anisotropic attraction forces appear as the solution of the full set of elasticity equations (see ref.[13]). Alternative approach to take into account elasticity potentials was proposed in ref.[14] and is based on the proper consideration of compatibility constraint caused by absence of a dislocation in the solid. Phenomenological aspects of the phase separation was discussed recently in the model of Coulomb frustrated phase transition [15, 16, 17].

Here we consider some aspects of the phase separation associated with different types of ordering of *charged* polarons. The formation of polaronic droplets in this case is due to competition of two types of interactions: the long range Coulomb repulsion and attraction generated by the deformation field. It is important to underline that if we consider the system of neutral polarons (without Coulomb repulsion), it shows a first order phase transition at

constant chemical potential, and is unstable with respect to global phase separation at fixed density[17]. Electron-phonon interaction may be short range and long range, depending on the type of phonons involved. In most of the cases we consider phonons of the molecular type, leading to short range forces. In some cases we consider long-range Fröhlich electron-phonon interaction and interaction with the strain.

2 Single polaron in the adiabatic approximation

Adiabatic theory of polarons was formulated many years ago [18, 19] and we briefly formulate here the main principles of adiabatic theory for the particular case of interaction with molecular vibrations (Holstein model). The central equation in the adiabatic theory is the Schrödinger equation for the electron in the external potential of the deformation field. In the discrete version it has the following form [20]:

$$-\sum_{\mathbf{m} \neq 0} t(\mathbf{m})[\psi_{\mathbf{n}}^k - \psi_{\mathbf{n}+\mathbf{m}}^k] + \sqrt{2}g\omega_0\varphi_{\mathbf{n}}\psi_{\mathbf{n}}^k = E_k\psi_{\mathbf{n}}^k. \quad (1)$$

Here $t(\mathbf{m})$ is hopping integral, $\psi_{\mathbf{n}}$ is electronic wave function on the site \mathbf{n} , $\varphi_{\mathbf{n}}$ is the deformation at the site \mathbf{n} , g is electron phonon coupling constant and ω_0 is phonon frequency, k describes quantum numbers of the problem. Important assumption of the adiabatic approximation is that deformation field is very slow and we assume that $\varphi_{\mathbf{n}}$ is time independent $\partial\varphi/\partial t = 0$ when we substitute it to the Schrödinger equation for electron. Therefore, $\omega_0 \rightarrow 0$ and $g^2 \rightarrow \infty$ but the product $g^2\omega_0 = E_p$ is finite and called polaron shift. The equation for $\varphi_{\mathbf{n}}$ has the form [20]:

$$\varphi_{\mathbf{n}} = -\sqrt{2}g|\psi_{\mathbf{n}}^0|^2 \quad (2)$$

Here $\psi_{\mathbf{n}}^0$ corresponds to the ground state solution of the Eq.(1). After substitution of the Eq.(2) to Eq.(1) we obtain:

$$-\sum_{\mathbf{m} \neq 0} t(\mathbf{m})[\psi_{\mathbf{n}}^k - \psi_{\mathbf{n}+\mathbf{m}}^k] - 2E_p|\psi_{\mathbf{n}}^0|^2\psi_{\mathbf{n}}^k = E_k\psi_{\mathbf{n}}^k. \quad (3)$$

As a result nonlinear Schrödinger equation (Eq.(3)) describes the ground state of the polaron. All excited states are the eigenvalues and eigenfunctions of the *linear* Schrödinger equation in the presence of the external field determined by the deformation field Eq.(2). Polaron energy is the sum of two contributions. The first is the energy of electron in the self-consistent potential well, determined by Eq.(3), and the second is the energy of the strain field φ itself $E_{pol} = E_0 + \omega_0 \sum_{\mathbf{n}} \varphi_{\mathbf{n}}^2/2$. The polaron energy is presented in the Fig.1 as a

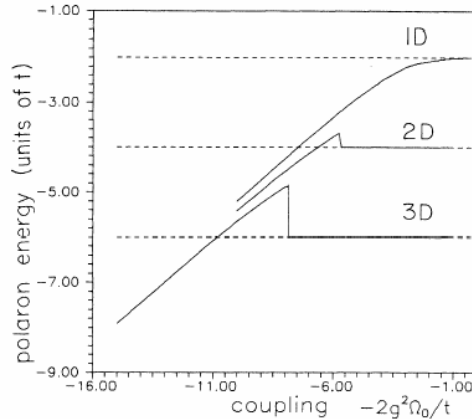


Fig. 1. Polaron energy as a function of coupling constant in 1D,2D and 3D cases. Dashed lines represent the energy of delocalized solution in 1D, 2D and 3D respectively

function of the dimensionless coupling constant $2g^2\omega_0/t$ in 1D, 2D and 3D cases.

There is very important difference between 1D and 2,3D cases. Polaron energy for 1D case is always less than the energy of the delocalized state (dashed line). Polaron is always stable in 1D. In 2D and 3D cases there is critical value of the coupling constant where first localized solution of Eq.(3) appears. It is interesting that the energy of the solution is higher than energy of the delocalized state. Therefore in 2D and 3D cases there is range of coupling constant where polaron is metastable. Delocalized solution is always stable in 3D case. Therefore, the barrier, which separates localized and delocalized states exists in the whole region of the coupling constants, where self-trapped solution exists. In 2D case the delocalized state is unstable at large value of the coupling constant. The barrier separating localized and delocalized states forms only in the restricted region of the coupling constant [20]. To demonstrate that we have plotted polaron energy as a function of its radius in 2D in the Fig.2. As it is clearly seen from this figure, barrier has disappeared at $g > g_{c3} = \sqrt{2\pi t/\omega_0}$ [20].

There are two types of non-adiabatic corrections to adiabatic polaron. The first is related to renormalization of local phonon modes. Fast motion of the electron within polaronic potential well leads to the shift of the local vibrational frequency:

$$\omega = \omega_0 [1 - zt^2/2(g^2\omega_0)^2]^{1/2} \quad (4)$$

here z is the number of nearest neighbors. This formula is valid in the strong coupling limit $g^2\omega_0 \gg t$ and when tunneling frequency of the polaron is much smaller than phonon frequency.

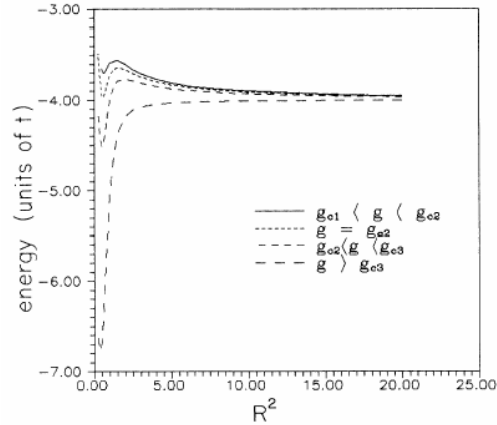


Fig. 2. Polaron energy as a function of radius in 2D. For $g > g_{c3}$ $\partial E_{pol}/\partial R < 0$. $g_{c1} = 1.69\sqrt{t/\omega_0}$, and $g_{c2} = 1.87\sqrt{t/\omega_0}$

Another type of correction is related to the restoration of translational symmetry (Goldstone mode) and describes polaron tunnelling and formation of the polaron band. This correction was calculated in the original paper of Holstein (Ref.[18]). Slightly improved formula was derived in [21]. In the adiabatic limit polaron tunnelling is exponentially suppressed $t_{eff} \propto \sqrt{E_p\omega_0} \exp(-g^2)$ (see Eq. (9) of the Ref.[21]) and should be smaller than phonon frequency ω_0 .

In the following we will neglect all nonadiabatic corrections. We will consider polaron as pure localized state, and all corrections which contain phonon frequency itself and tunnelling amplitude for polaron are neglected.

3 Strings in charge-transfer Mott insulators: effects of lattice vibrations and the Coulomb interaction

Here we prove that the Fröhlich electron-phonon interaction combined with the direct Coulomb repulsion does not lead to charge segregation like strings in doped narrow-band insulators, both in the nonadiabatic and adiabatic regimes. However, this interaction significantly reduces the Coulomb repulsion, which might allow much weaker antiferromagnetic and/or short-range electron-phonon interactions to segregate charges in the doped insulators, as suggested by previous studies [4, 5, 11].

To begin with, we consider a generic Hamiltonian, including, respectively, the kinetic energy of carriers, the Fröhlich electron-phonon interaction, phonon energy, and the Coulomb repulsion as

$$\begin{aligned}
 H = & \sum_{i \neq j} t(\mathbf{m} - \mathbf{n}) \delta_{s,s'} c_i^\dagger c_j + \sum_{\mathbf{q}, i} \omega_{\mathbf{q}} n_i [u_i(\mathbf{q}) d_{\mathbf{q}} + H.c.] \\
 & + \sum_{\mathbf{q}} \omega_{\mathbf{q}} (d_{\mathbf{q}}^\dagger d_{\mathbf{q}} + 1/2) + \frac{1}{2} \sum_{i \neq j} V(\mathbf{m} - \mathbf{n}) n_i n_j
 \end{aligned} \quad (5)$$

with bare hopping integral $t(\mathbf{m})$, and matrix element of the electron-phonon interaction

$$u_i(\mathbf{q}) = \frac{1}{\sqrt{2N}} \gamma(\mathbf{q}) e^{i\mathbf{q} \cdot \mathbf{m}}. \quad (6)$$

Here $i = (\mathbf{m}, s)$, $j = (\mathbf{n}, s')$ include site \mathbf{m}, \mathbf{n} and spin s, s' quantum numbers, $n_i = c_i^\dagger c_i$, $c_i, d_{\mathbf{q}}$ are the electron (hole) and phonon operators, respectively, and N is the number of sites. At large distances (or small q) one finds

$$\gamma(\mathbf{q})^2 \omega_{\mathbf{q}} = \frac{4\pi e^2}{\kappa q^2}, \quad (7)$$

and

$$V(\mathbf{m} - \mathbf{n}) = \frac{e^2}{\epsilon_\infty |\mathbf{m} - \mathbf{n}|}. \quad (8)$$

The phonon frequency $\omega_{\mathbf{q}}$ and the static and high-frequency dielectric constants in $\kappa^{-1} = \epsilon_\infty^{-1} - \epsilon_0^{-1}$ are those of the host insulator ($\hbar = c = 1$).

In the adiabatic limit one can apply a discrete version of the continuous nonlinear equation [22] proposed for the Holstein model (Eq.(1)), extended to the case of the deformation and Fröhlich interactions in Ref. [11, 9, 10]. Applying the Hartree approximation for the Coulomb repulsion, the single-particle wave-function, $\psi_{\mathbf{n}}$ (the amplitude of the Wannier state $|\mathbf{n}\rangle$) obeys the following equation

$$- \sum_{\mathbf{m} \neq 0} t(\mathbf{m}) [\psi_{\mathbf{n}} - \psi_{\mathbf{n}+\mathbf{m}}] - e\phi_{\mathbf{n}} \psi_{\mathbf{n}} = E\psi_{\mathbf{n}}. \quad (9)$$

The potential $\phi_{\mathbf{n},k}$ acting on a fermion k at the site \mathbf{n} is created by the polarization of the lattice $\phi_{\mathbf{n},k}^l$ and by the Coulomb repulsion with the other $M - 1$ fermions, $\phi_{\mathbf{n},k}^c$,

$$\phi_{\mathbf{n},k} = \phi_{\mathbf{n},k}^l + \phi_{\mathbf{n},k}^c. \quad (10)$$

Both potentials satisfy the discrete Poisson equation as

$$\kappa \Delta \phi_{\mathbf{n},k}^l = 4\pi e \sum_{p=1}^M |\psi_{\mathbf{n},p}|^2, \quad (11)$$

and

$$\epsilon_\infty \Delta \phi_{\mathbf{n},k}^c = -4\pi e \sum_{p=1, p \neq k}^M |\psi_{\mathbf{n},p}|^2, \quad (12)$$

with $\Delta\phi_{\mathbf{n}} = \sum_{\mathbf{m}}(\phi_{\mathbf{n}} - \phi_{\mathbf{n}+\mathbf{m}})$. Differently from Ref. [9] we include the Coulomb interaction in Pekar's functional J [22], describing the total energy, in a selfconsistent manner using the Hartree approximation, so that[10]

$$\begin{aligned}
J = & - \sum_{\mathbf{n}, \mathbf{p}, \mathbf{m} \neq 0} \psi_{\mathbf{n}, \mathbf{p}}^* t(\mathbf{m}) [\psi_{\mathbf{n}, \mathbf{p}} - \psi_{\mathbf{n}+\mathbf{m}, \mathbf{p}}] \\
& - \frac{2\pi e^2}{\kappa} \sum_{\mathbf{n}, \mathbf{p}, \mathbf{m}, \mathbf{q}} |\psi_{\mathbf{n}, \mathbf{p}}|^2 \Delta^{-1} |\psi_{\mathbf{m}, \mathbf{q}}|^2 \\
& + \frac{2\pi e^2}{\epsilon_{\infty}} \sum_{\mathbf{n}, \mathbf{p}, \mathbf{m}, \mathbf{q} \neq \mathbf{p}} |\psi_{\mathbf{n}, \mathbf{p}}|^2 \Delta^{-1} |\psi_{\mathbf{m}, \mathbf{q}}|^2.
\end{aligned} \tag{13}$$

If we assume, following Ref. [11] that the single-particle function of a fermion trapped in a string of the length N is a simple exponent, $\psi_n = N^{-1/2} \exp(ikn)$ with the periodic boundary conditions, then the functional J is expressed as $J = T + U$, where $T = -2t(N-1) \sin(\pi M/N) / [N \sin(\pi/N)]$ is the kinetic energy (for an *odd* number M of spinless fermions), proportional to t , and

$$U = -\frac{e^2}{\kappa} M^2 I_N + \frac{e^2}{\epsilon_{\infty}} M(M-1) I_N, \tag{14}$$

corresponds to the polarisation and the Coulomb energies. Here the integral I_N is given by

$$\begin{aligned}
I_N = & \frac{\pi}{(2\pi)^3} \int_{-\pi}^{\pi} dx \int_{-\pi}^{\pi} dy \int_{-\pi}^{\pi} dz \frac{\sin(Nx/2)^2}{N^2 \sin(x/2)^2} \\
& \times (3 - \cos x - \cos y - \cos z)^{-1}.
\end{aligned} \tag{15}$$

I_N has the following asymptotic [10]:

$$I_N = \frac{1.31 + \ln N}{N}, \tag{16}$$

The asymptotic is derived also analytically at large N by the use of the fact that $\sin(Nx/2)^2 / (2\pi N \sin(x/2)^2)$ can be replaced by a δ - function. If we split the first (attractive) term in Eq.(14) into two parts by replacing M^2 for $M + M(M-1)$, it becomes clear that the net interaction between polarons remains repulsive in the adiabatic regime because $\kappa > \epsilon_{\infty}$. Hence, there are no strings within the Hartree approximation for the Coulomb interaction. Strong correlations do not change this conclusion. Indeed, if we take the Coulomb energy of spinless one-dimensional fermions comprising both Hartree and exchange terms as

$$E_C = \frac{e^2 M(M-1)}{N \epsilon_{\infty}} [0.916 + \ln M], \tag{17}$$

the polarisation and Coulomb energy per particle becomes (for large $M \gg 1$)

$$U/M = \frac{e^2 M}{N \epsilon_{\infty}} [0.916 + \ln M - \alpha(1.31 + \ln N)], \tag{18}$$

where $\alpha = 1 - \epsilon_\infty/\epsilon_0 < 1$. Minimising this energy with respect to the length of the string N we find

$$N = M^{1/\alpha} \exp(-0.31 + 0.916/\alpha), \quad (19)$$

and

$$(U/M)_{min} = -\frac{e^2}{\kappa} M^{1-1/\alpha} \exp(0.31 - 0.916/\alpha). \quad (20)$$

Hence, the potential energy per particle increases with the number of particles so that the energy of M well separated polarons is lower than the energy of polarons trapped in a string no matter whether they are correlated or not. The opposite conclusion of Ref. [9] originates in an incorrect approximation of the integral $I_N \propto N^{0.15}/N$. The correct asymptotic result is $I_N = \ln(N)/N$.

One can argue [9] that a finite kinetic energy (t) can stabilise a string of a finite length. Unfortunately, this is not correct either. We performed exact (numerical) calculations of the total energy $E(M, N)$ of M spinless fermions in a string of the length N including both kinetic and potential energy with the typical values of $\epsilon_\infty = 5$ and $\epsilon_0 = 30$. The local energy minima (per particle) in the string of the length $1 \leq N \leq 69$ containing $M \leq N/2$ particles are presented in the Table 1. Strings with even fermion numbers carry a finite current and hence the local minima are found for odd M . In the extreme wide band regime with t as large as 1 eV the global string energy minimum is found at $M = 3, N = 25$ ($E = -2.1167$ eV), and at $M = 3, N = 13$ for $t = 0.5$ eV ($E = -1.2138$ eV). However, this is *not* the ground state energy in both cases. The energy of well separated $d \geq 2$ -dimensional polarons is well below, less than $-2dt$ per particle (i.e. -6 eV in the first case and -3 eV in the second one in the three dimensional cubic lattice, and -4 eV and -2 eV, respectively, in the two-dimensional square lattice). This argument is applied for any values of $\epsilon_0, \epsilon_\infty$ and t . As a result we have proven that strings are impossible with the Fröhlich interaction alone contrary to the erroneous Ref. [9].

Table 1. $E(M, N)$ for $t = 1$ eV and $t = 0.5$ eV

		$t = 1\text{eV}$		$t = 0.5\text{eV}$	
M	N	E(M,N)	N	E(M,N)	
1	11	-2.0328	3	-1.1919	
3	25	-2.1167	13	-1.2138	
5	42	-2.1166	25	-1.1840	
7	61	-2.1127	40	-1.1661	

The Fröhlich interaction is, of course, not the only electron-phonon interaction in ionic solids. As discussed in Ref. [23], any short range electron-phonon interaction, like, for example, the Jahn-Teller (JT) distortion can overcome

the residual weak repulsion of Fröhlich polarons to form small bipolarons. At large distances small nonadiabatic bipolarons weakly repel each other due to the long-range Coulomb interaction, four times of that of polarons, Eq.(9). Hence, they form a liquid state [23], or bipolaronic-polaronic crystal-like structures [24] depending on their effective mass and density. The fact, that the Fröhlich interaction almost nullifies the Coulomb repulsion in oxides justifies the use of the Holstein-Hubbard model [25, 26]. The ground state of the 1D Holstein-Hubbard model is a liquid of intersite bipolarons with a significantly reduced mass (compared with the on-site bipolaron) as shown recently [27]. The bound states of three or more polarons are not stable in this model, thus ruling out phase separation. However, the situation might be different if the antiferromagnetic [4, 5] and JT interaction[6] or any other short (but finite) range electron-phonon interaction are strong enough. Due to long-range nature of the Coulomb repulsion the length of a string should be finite (see, also Ref.[11, 10, 28]).

To summarize we conclude that there are no strings in ionic doped insulators with the Fröhlich interaction alone. Depending on their density and mass polarons remain in a liquid state or Wigner crystal. On the other hand the short-range electron-phonon and/or antiferromagnetic interactions might provide a liquid bipolaronic state and/or charge segregation (strings of a finite length) since the long-range Fröhlich interaction significantly reduces the Coulomb repulsion in highly polarizable ionic insulators.

4 Ordering of charged polarons: Lattice gas model

In this section we consider macroscopic system of polarons in the thermodynamic limit. To underline nontrivial geometry of the phase separation we consider two-fold degenerate electronic states which interact with nonsymmetric deformation field. In our derivation we follow particular model for high- T_c superconductors. Nevertheless the results are general enough and are applicable to many Jahn-Teller systems.

Recently we formulated the model[29] where we suggested that interaction of a two-fold degenerate electronic state with fully symmetric of the small group τ_1 phonon modes at a finite wave-vector can lead to a local nonsymmetric deformation and short-length scale charge segregation in high- T_c materials. Here we reduced the proposed model to the lattice gas model[17] and showed that the model indeed displays phase separation, which may occur in the form of stripes or clusters depending on the anisotropy of the short range attraction between localized carriers[17]. We also generalized the model taking into account interaction of the Jahn-Teller centers via elasticity induced field[17]. We showed that the model without Coulomb repulsion displays a first order phase transition at a constant chemical potential. When the number of particles is fixed, the system is unstable with respect to the global phase separation below certain critical temperature. In the presence of

the Coulomb repulsion global phase separation becomes unfavorable due to a large contribution to the energy from long range Coulomb interaction. The system shows mesoscopic phase separation where the size of charged regions is determined by the competition between the energy gain due to ordering and energy cost due to breaking of the local charge neutrality. Since the short range attraction is anisotropic the phase separation may be in the form of short segments or/and stripes.

Let us start with the construction of a real-space Hamiltonian which couples 2-fold degenerate electronic states (or near-degenerate states) with optical phonons of τ_1 symmetry. Two-fold degeneracy is essential because in that case formation of the polaronic complexes leads to reduction not only of translational symmetry but also reduction of the point group symmetry. Since the Hamiltonian needs to describe a 2-fold degenerate system, the 2-fold degenerate states - for example the two E_u states corresponding to the planar hybridized Cu $d_{x^2-y^2}$, O p_x and p_y orbitals, or the E_u and E_g states of the apical O - are written in the form of Pauli matrices σ_i . Taking into account that the states are real, the Pauli matrices which describe transitions between the levels transform as A_{1g} ($k_x^2 + k_y^2$) for σ_0 , B_{1g} ($k_x^2 - k_y^2$) for σ_3 , B_{2g} ($k_x k_y$) for σ_1 , and A_{2g} (s_z) for σ_2 representations respectively. Collecting terms together by symmetry we can construct *effective* electron-spin-lattice interaction Hamiltonian given in the Ref.[29]. Here we consider a simplified version of the JT model Hamiltonian [29], taking only the deformation of the B_{1g} symmetry:

$$H_{JT} = g \sum_{\mathbf{n}, \mathbf{l}} \sigma_{3,1} f(\mathbf{n}) (b_{\mathbf{l}+\mathbf{n}}^\dagger + b_{\mathbf{l}+\mathbf{n}}), \quad (21)$$

here the Pauli matrix $\sigma_{3,1}$ describes two components of the electronic doublet, and $f(\mathbf{n}) = (n_x^2 - n_y^2) f_0(n)$ where $f_0(n)$ is a symmetric function describing the range of the interaction. For simplicity we omit the spin index in the sum. The model could be easily reduced to a lattice gas model[17]. Let us introduce the classical variable $\Phi_{\mathbf{i}} = \langle b_{\mathbf{i}}^\dagger + b_{\mathbf{i}} \rangle / \sqrt{2}$ and minimize the energy as a function of $\Phi_{\mathbf{i}}$ in the presence of the harmonic term $\omega \sum_{\mathbf{i}} \Phi_{\mathbf{i}}^2 / 2$. We obtain the deformation, corresponding to the minimum of energy,

$$\Phi_{\mathbf{i}}^{(0)} = -\sqrt{2}g/\omega \sum_{\mathbf{n}} \sigma_{3,1+\mathbf{n}} f(\mathbf{n}). \quad (22)$$

Substituting $\Phi_{\mathbf{i}}^{(0)}$ into the Hamiltonian (1) and taking into account that the carriers are charged we arrive at the lattice gas model. We use a pseudospin operator $S = 1$ to describe the occupancies of the two electronic levels n_1 and n_2 . Here $S^z = 1$ corresponds to the state with $n_1 = 1$, $n_2 = 0$, $S_i^z = -1$ to $n_1 = 0$, $n_2 = 1$ and $S_i^z = 0$ to $n_1 = n_2 = 0$. Simultaneous occupancy of both levels is excluded due to a high on-site Coulomb repulsion energy. The Hamiltonian in terms of the pseudospin operator is given by[17]

$$H_{LG} = \sum_{\mathbf{i}, \mathbf{j}} (-V_l(\mathbf{i} - \mathbf{j}) S_{\mathbf{i}}^z S_{\mathbf{j}}^z + V_c(\mathbf{i} - \mathbf{j}) Q_{\mathbf{i}} Q_{\mathbf{j}}), \quad (23)$$

where $Q_{\mathbf{i}} = (S_{\mathbf{i}}^z)^2$. $V_c(\mathbf{n}) = e^2/\epsilon_0 a(n_x^2 + n_y^2)^{1/2}$ is the Coulomb potential, e is the charge of electron, ϵ_0 is the static dielectric constant and a is the effective unit cell period. The anisotropic short range attraction potential is given by $V_l(\mathbf{n}) = g^2/\omega \sum_{\mathbf{m}} f(\mathbf{m})f(\mathbf{n}+\mathbf{m})$. The attraction in this model is generated by the interaction of electrons with optical phonons. The radius of the attraction force is determined by the radius of the electron-phonon interaction and the dispersion of optical phonons[10].

A similar model can be formulated in the limit of continuous media[17]. The deformation is characterized by the components of the strain tensor. For the two dimensional case we can define 3 components of the strain tensor: $e_1 = u_{xx} + u_{yy}$, $\epsilon = u_{xx} - u_{yy}$ and $e_2 = u_{xy}$ transforming as the A_{1g} , B_{1g} and B_{2g} representations of the D_{4h} group respectively. These components of the tensor are coupled linearly with the two-fold degenerate electronic state which transforms as the E_g or E_u representation of the point group. Similarly to the case of previously considered interaction with optical phonons we keep the interaction with the deformation ϵ of the B_{1g} symmetry only. The Hamiltonian without the Coulomb repulsion term has the form:

$$H = g \sum_{\mathbf{i}} S_{\mathbf{i}}^z \epsilon_{\mathbf{i}} + \frac{1}{2} (A_1 \epsilon_{1,\mathbf{i}}^2 + A_2 \epsilon_{\mathbf{i}}^2 + A_3 \epsilon_{3,\mathbf{i}}^2), \quad (24)$$

where A_j are corresponding components of the elastic modulus tensor. The components of the strain tensor are not independent [30, 14] and satisfy the compatibility condition:

$$\nabla^2 e_1(\mathbf{r}) - 4\partial^2 e_2(\mathbf{r})/\partial x \partial y = (\partial^2/\partial x^2 - \partial^2/\partial y^2)\epsilon(\mathbf{r})$$

The compatibility condition leads to a long range anisotropic interaction between polarons. The Hamiltonian in the reciprocal space has the form:

$$H = g \sum_{\mathbf{k}} S_{\mathbf{k}}^z \epsilon_{\mathbf{k}} + (A_2 + A_1 U(\mathbf{k})) \frac{\epsilon_{\mathbf{k}}^2}{2}. \quad (25)$$

The Fourier transform of the potential is given by:

$$U(\mathbf{k}) = \frac{(k_x^2 - k_y^2)^2}{k^4 + 8(A_1/A_3)k_x^2 k_y^2}. \quad (26)$$

By minimizing the energy with respect to $\epsilon_{\mathbf{k}}$ and taking into account the long-range Coulomb repulsion we again derive Eq.(23). The anisotropic interaction potential $V_l(\mathbf{n}) = -\sum_{\mathbf{k}} \exp(i\mathbf{k} \cdot \mathbf{n}) \frac{g^2}{2(A_2 + A_1 U(\mathbf{k}))}$ is determined by the interaction with the classical deformation and is long-range. It decays as $1/r^2$ at large distances in 2D. Since at large distances the attraction forces decay faster then the Coulomb repulsion forces the attraction can overcome the Coulomb repulsion at short distances, leading to a mesoscopic phase separation.

Irrespective of whether the resulting interaction between polarons is generated by acoustic or optical phonons the main physical picture remains the

same. In both cases there is an anisotropic attraction between polarons on short distances. The interaction could be either ferromagnetic or antiferromagnetic in terms of the pseudospin operators depending on mutual orientation of the orbitals. Without losing generality we assume that $V(\mathbf{n})$ is nonzero only for the nearest neighbors.

Our aim is to study the model (Eq.(23)) at constant average density,

$$n = \frac{1}{N} \sum_{\mathbf{i}} Q_{\mathbf{i}}, \quad (27)$$

where N is the total number of sites. However, to clarify the physical picture it is more appropriate to perform calculations with a fixed chemical potential first by adding the term $-\mu \sum_{\mathbf{i}} Q_{\mathbf{i}}$ to the Hamiltonian (23).

Models such as Eq.(23) without the long-range forces, were studied many years ago on the basis of the molecular-field approximation in the Bragg-Williams formalism [31, 32]. The mean-field equations for the particle density n and the pseudospin magnetization $M = \frac{1}{N} \sum_{\mathbf{i}} S_{\mathbf{i}}^z$ have the form[31]:

$$M = \frac{2 \sinh(2zV_l M/k_B T)}{\exp(-\mu/k_B T) + 2 \cosh(2zV_l M/k_B T)} \quad (28)$$

$$n = \frac{2 \cosh(2zV_l M/k_B T)}{\exp(-\mu/k_B T) + 2 \cosh(2zV_l M/k_B T)} \quad (29)$$

here $z = 4$ is the number of the nearest neighbours for a square lattice in 2D and k_B is the Boltzman constant. A phase transition to an ordered state with finite M may be of either first or second order, depending on the value of μ . For the physically important case $-2zV_l < \mu < 0$, ordering occurs as a result of the first order phase transition. The two solutions of Eqs.(28,29) with $M = 0$ and $M \neq 0$ correspond to two different minima of the free energy. The temperature of the phase transition T_{crit} is determined by the condition: $F(M = 0, \mu, T) = F(M, \mu, T)$ where M is the solution of Eq. (28). When the number of particles is fixed (Eq.(29)), the system is unstable with respect to global phase separation below T_{crit} . As a result, at fixed n two phases coexist with $n_0 = n(M = 0, \mu, T)$ and $n_M = n(M, \mu, T)$, resulting in a liquid-gas-like phase diagram (Fig.3).

To investigate the effects of the long range-forces, we performed Monte Carlo simulations on the system (23)[17]. The simulations were performed on a square lattice with dimensions up to $L \times L$ sites with $10 \leq L \leq 100$ using a standard Metropolis algorithm[33] in combination with simulated annealing[34]. At constant n one Monte Carlo step included a single update for each site with nonzero Q_i , where the trial move consisted from setting $S_z = 0$ at the site with nonzero Q_i and $S_z = \pm 1$ at a randomly selected site with zero Q_i . A typical simulated annealing run consisted from a sequence of Monte Carlo simulations at different temperatures. At each temperature the equilibration phase ($10^3 - 10^6$ Monte Carlo steps) was followed by the averaging phase with the same or greater number of Monte Carlo steps. Observables

were measured after each Monte Carlo step during the averaging phase only. For $L \gtrsim 20$ we observe virtually no dependence of the results on the system size.

Comparing the Monte Carlo results in the absence of Coulomb repulsion shown by t_{crit} in Fig. 3 with MF theory we find the usual reduction of t_{crit} due to fluctuations in 2D by a factor of ~ 2 .

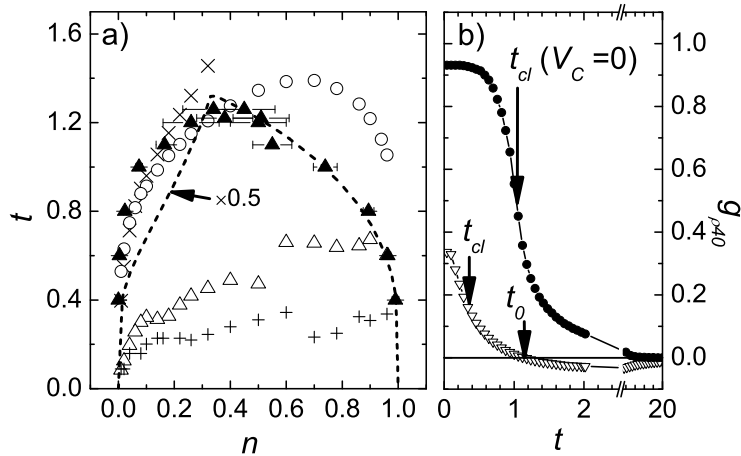


Fig. 3. a) The phase diagram generated by H_{JT} (23) with, and without the Coulomb repulsion (CR). The dashed line is the MF critical temperature, while the full triangles (\blacktriangle) represent the Monte Carlo critical temperature, t_{crit} , without CR. The open circles (\circ) represent t_{cl} , without CR. The open triangles (\triangle) represent t_{cl} while the diagonal crosses (\times) represent the onset of clustering, t_0 , in the presence of CR. The cluster-ordering temperature (see text), t_{co} , (also incl. CR) is shown as crosses ($+$). The size of the symbols corresponds to the error bars. b) Typical temperature dependencies of the nearest neighbor density correlation function $g_{\rho L}$ for $n = 0.18$ in the absence of CR (\bullet) and in the presence of CR (∇). Arrows indicate the characteristic temperatures.

Next, we include the Coulomb interaction $V_c(r)$. We use open boundary conditions to avoid complications due to the long range Coulomb forces and ensure overall electroneutrality by adding a uniformly charged background electrostatic potential (jellium) to Eq. (23). The short range potential $v_l(\mathbf{i}) = V_l(\mathbf{i})\epsilon_0 a/e^2$ was taken to be nonzero only for $|\mathbf{i}| < 2$ and is therefore specified only for nearest, and next-nearest neighbours as $v_l(1, 0)$ and $v_l(1, 1)$ respectively.

The anisotropy of the short range potential has a profound influence on the particle ordering. We can see this if we fix $v_l(1, 0) = -1$, at a density $n = 0.2$ and vary the next-nearest neighbour potential $v_l(1, 1)$ in the range from -1 to 1 . When $v_l(1, 1) < 0$, the attraction is "ferrodistortive" in all directions, while for positive $v_l(1, 1) > 0$ the interaction is "antiferrodistortive" along the

diagonals. The resulting clustering and ordering of clusters at $t = 0.04$ is shown in Fig. 4a). As expected, a more symmetric attraction potential leads to the formation of more symmetric clusters. On the other hand, for $v_l(1, 1) = 1$, the "antiferrodistortive" interaction along diagonals prevails, resulting in diagonal stripes.

In the temperature region where clusters partially order the heat capacity ($c_L = \partial \langle E \rangle_L / \partial T$ where E is the total energy) displays the peak at t_{co} . The peak displays no scaling with L indicating that no long range ordering of clusters appears. Inspection of the particle distribution snapshots at low temperatures (Fig. 4a) reveals that finite size domains form. Within domains the clusters are perfectly ordered. The domain wall dynamics seems to be much slower than our Monte Carlo simulation timescale preventing domains to grow. The effective L is therefore limited by the domain size. This explains the absence of the scaling and clear evidence for a phase transition near t_{co} .

We now focus on the shape of the short range potential which promotes the formation of stripes shown in Fig. 4a). We set $v_l(1, 0) = -1$ and $v_l(1, 1) = 0$ and study the density dependence. Since the inclusion of the Coulomb interaction completely suppresses the first order phase transition at t_{crit} , we measure the nearest neighbor density correlation function $g_{\rho L} = \frac{1}{4n(1-n)L^2} \sum_{|\mathbf{m}|=1} \langle \sum_{\mathbf{i}} (Q_{\mathbf{i}+\mathbf{m}} - n)(Q_{\mathbf{i}} - n) \rangle_L$ to detect clustering. Here $\langle \rangle_L$ represents the Monte Carlo average. We define a dimensionless temperature $t_{cl} = k_B T_{cl} \epsilon_0 a / e^2$ as the characteristic crossover temperature related to the formation of clusters at which $g_{\rho L}$ rises to 50% of its low temperature value. The dependence of t_{cl} on the density n is shown in the phase diagram in Fig. 3. Without Coulomb repulsion $V_c(r)$, t_{cl} follows t_{crit} , as expected. The addition of Coulomb repulsion $V_C(r)$ results in a significant decrease of t_{cl} and suppression of clustering. At low densities we can estimate the onset for cluster formation by the temperature, t_0 , at which $g_{\rho L}$ becomes positive. It is interesting to note that t_0 almost coincides with the t_{crit} line at low n (Fig. 3).

To illustrate this behaviour, in Fig. 4b) we show snapshots of the calculated Monte Carlo particle distributions at two different temperatures for different densities. The growth and ordering of clusters with decreasing temperature is clearly observed. At low n , the particles form mostly pairs with some short stripes. With further increasing density, quadruples gradually replace pairs, then longer stripes appear, mixed with quadruples, etc.. At the highest density, stripes prevail forming a labyrinth-like pattern. The density correlation function shows that the correlation length increases with doping, but long range order is never achieved (in contrast to the case without V_c). Note that while locally there is no four-fold symmetry the overall correlation function still retains 4-fold symmetry.

To get further insight in the cluster formation we measured the cluster-size distribution [17]. In Fig. 5 we present the temperature and density dependence of the cluster-size distribution function $x_L(j) = \langle N_p(j) \rangle_L / (nL^2)$, where $N_p(j)$ is the total number of particles within clusters of size j . At the highest tem-

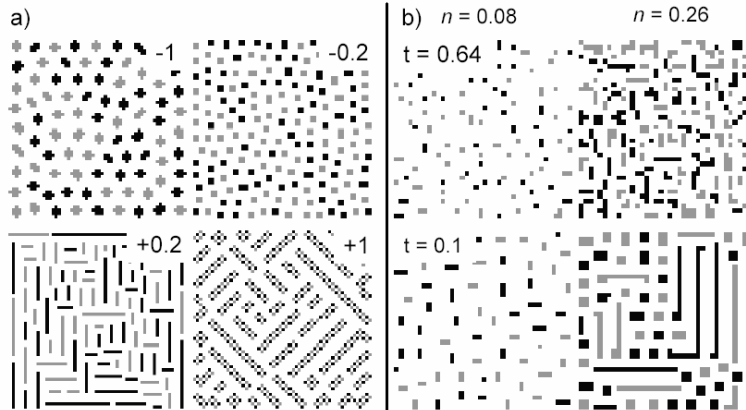


Fig. 4. a) Snapshots of clusters ordering at $t = 0.04$, $n = 0.2$ and $v_l(1,0) = -1$ for different diagonal $v_l(1,1)$ (given in each figure). Grey and black dots represent particles clusters in state $S_i^z = 1$ and states $S_i^z = -1$ respectively. The preference for even-particle-number clusters in certain cases is clearly observed, for example for $v_l(1,1) = -0.2$. b) Snapshots of the particle distribution for two densities at two different temperatures $t = 0.64$ and $t = 0.1$ respectively.

perature $x_L(j)$ is close to the distribution expected for the random ordering. As the temperature is decreased, the number of larger clusters starts to increase at the expense of single particles. Remarkably, as the temperature is further reduced, clusters of certain size start to prevail. This is clearly seen at higher densities (Fig.3). Depending on the density, the prevailing clusters are pairs up to $n \approx 0.2$, quadruples for $0.1 \lesssim n \lesssim 0.3$ etc.. We note that for a large range of $v_l(1,0)$, the system prefers clusters with an even number of particles. Odd particle-number clusters can also form, but have a much narrower parameter range of stability. The preference to certain cluster sizes becomes clearly apparent only at temperatures lower than t_{cl} , and the transition is not abrupt but gradual with the decreasing temperature. Similarly, with increasing density changes in textures also indicate a series of crossovers.

The results of the Monte Carlo simulation[17] presented above allow a quite general interpretation in terms of the kinetics of first order phase transitions[35]. Let us assume that a single cluster of ordered phase with radius R appears. As was discussed in [7, 29], the energy of the cluster is determined by three terms: $\epsilon = -F\pi R^2 + \alpha\pi R + \gamma R^3$. The first term is the energy gain due to the ordering phase transition where F is the energy difference between the two minima in the free energy density. The second term is the surface energy parameterized by α , and the third term is the Coulomb energy, parameterized by γ . If $\alpha < \pi F/3\gamma$, ϵ has a well defined minimum at $R = R_0$ corresponding to the optimal size of clusters in the system. Of course, these clusters are also interacting among themselves via Coulomb and strain

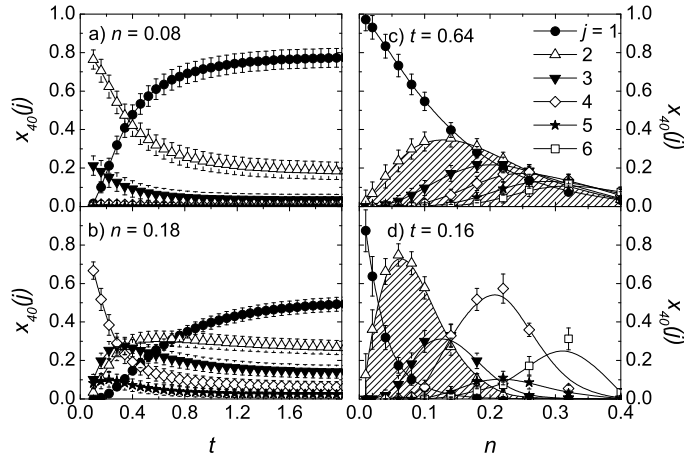


Fig. 5. The temperature dependence of the cluster-size distribution function $x_L(j)$ (for the smallest cluster sizes) as a function of temperature at two different average densities $n = 0.08$ (a) and $n = 0.18$ (b). $x_L(j)$ as a function of n at the temperature between t_0 and t_{cl} (c), and near t_{co} (d). The ranges of the density where pairs prevail are very clearly seen in (d). Error bars represent the standard deviation.

forces, which leads to cluster ordering or freezing of cluster motion at low temperatures as shown by the Monte Carlo simulations.

We conclude that a model with only anisotropic JT strain and a long-range Coulomb interaction indeed is unstable with respect to the short scale phase separation and gives rise to a remarkably rich phase diagram including pairs, stripes and charge- and orbital- ordered phases, of clear relevance to oxides. The energy scale of the phenomena is defined by the parameters used in H_{JT-C} (23). For example, using the measured value $\epsilon_0 \simeq 40$ [36] for La_2CuO_4 , we estimate $V_c(1, 0) = 0.1$ eV, which is also the typical energy scale of the "pseudogap" in the cuprates. The robust prevalence of the paired state in a wide region of parameters (Fig. 5 c,d) is particularly interesting from the point of view of superconductivity. A similar situation occurs in manganites and other oxides with the onset of a conductive state at the threshold of percolation, but different textures are expected to arise due to different magnitude (and anisotropy) of $V_l(\mathbf{n})$, and static dielectric constant ϵ_0 in the different materials[37].

5 Coulomb frustrated first order phase transition

As it is stated in the previous section uncharged JT polarons have the tendency to ordering. The ordering transition is a phase transition of the first order. At the fixed density of polarons the system is unstable with respect to the global phase separation. The global phase separation is frustrated by charg-

ing effects leading to short-scale phase separation. Therefore the results of the Monte-Carlo simulation of the model (23) allow general model independent interpretation. Let us consider the classical free energy density corresponding to the first order phase transition:

$$F_1 = ((t - 1) + (\eta^2 - 1)^2)\eta^2 \quad (30)$$

Here $t = (T - T_c)/(T_0 - T_c)$ is dimensionless temperature. At $t = 4/3$ ($T = T_0 + (T_0 - T_c)/3$) the nontrivial minimum in the free energy appears. At $t = 1$ ($T = T_0$) the first order phase transition occurs, but the trivial solution $\eta = 0$ corresponds to the metastable phase. At $t = 0$ ($T = T_c$) trivial solution becomes unstable. In order to study the case of Coulomb frustrated phase transition we have to add coupling of the order parameter to local charge density. Our order parameter describes sublattice magnetization and therefore only square of the order parameter may be coupled to the local charge density ρ :

$$F_{coupl} = -\alpha\eta^2\rho \quad (31)$$

The total free energy density should contain the gradient term and the electrostatic energy:

$$F_{grad} + F_{el} = C(\nabla\eta)^2 + \frac{K}{2}[\rho(\mathbf{r}) - \bar{\rho}] \int d\mathbf{r}' [\rho(\mathbf{r}') - \bar{\rho}]/|\mathbf{r} - \mathbf{r}'| \quad (32)$$

Here we write $\bar{\rho}$ explicitly to take into account global electroneutrality. Total free energy Eqs.(30-32) should be minimized at fixed t and $\bar{\rho}$.

Let us demonstrate that Coulomb term leads to the phase separation in the 2D case. Minimization of F with respect to the charge density $\rho(\mathbf{r})$ leads to the following equation:

$$-\alpha\nabla_{3D}^2\eta^2 = 4\pi K[\rho(\mathbf{r}) - \bar{\rho}]d\delta(z) \quad (33)$$

here we write explicitly that density $\rho(\mathbf{r})$ depends only on 2D vector \mathbf{r} and introduce layer thickness d , to preserve correct dimensionality. Solving this equation by applying the Furrier transform and substituting the solution back to the free energy density we obtain:

$$F = F_1 - \alpha\eta^2\bar{\rho} + C(\nabla\eta)^2 - \frac{\alpha^2}{8\pi^2 K d} \int d\mathbf{r}' \frac{\nabla(\eta(\mathbf{r})^2)\nabla(\eta(\mathbf{r}')^2)}{|\mathbf{r} - \mathbf{r}'|} \quad (34)$$

As a results the free energy functional is similar to the case of the first order phase transition with shifted critical temperature due to the presence of the term $\alpha\eta^2\bar{\rho}$ and nonlocal gradient term of higher order.

To demonstrate that uniform solution has higher energy then nonhomogeneous solution we make Fourier transform of the gradient term:

$$F_{grad} \propto Ck^2|\eta_{\mathbf{k}}|^2 - \frac{\alpha^2 k |(\eta^2)_{\mathbf{k}}|^2}{4\pi K d} \quad (35)$$

here $\eta_{\mathbf{k}}$ and $(\eta^2)_{\mathbf{k}}$ are Fourier components of the order parameter and square of the order parameter respectively. If we assume that the solution is uniform i.e. $\eta_0 \neq 0$ and $(\eta^2)_0 \neq 0$ small nonuniform corrections to the solution reduces the free energy at small \mathbf{k} , where second term dominates.

Proposed free energy functional is similar to that proposed in the Ref.[16]. The important difference is that in our case the charge is coupled to the square of the order parameter and it plays the role of local temperature, while in the case of Ref.[16] there is linear coupling of the charge to the order parameter. Charge in that case plays the role of the external field. Moreover, contrary to the case of Ref[16] where charge is accumulated near *domain walls*, in our case charge is accumulated near *interphase boundaries*.

6 Conclusion

We have demonstrated that anisotropic interaction between Jahn-Teller centers generated by optical and/or acoustical phonons leads in the presence of the long range Coulomb repulsion to the short scale phase separation. Topology of texturing differs from charged bubbles to oriented charged stripes depending on the anisotropy of short range potential. On the phenomenological level inhomogeneous phase with charged regions appears due to tendency of the system of polarons to global phase separation, while global phase separation is frustrated by the long-range Coulomb forces. Effectively this system may be described by standard Landau functional with nonlocal long-range gradient term.

References

1. T. Egami et al., J supercond, **13**, 709 (2000); J. Tranquada et al., Nature **375**, 561 (1995).
2. A. Bianconi et al., Phys. Rev. Lett. **76**, 3412 (1996).
3. H.A. Mook and F. Dogan Nature, **401**, 145 (1999)
4. J. Zaanen, O Gunnarsson, Phys. Rev. B, **40**, 7391 (1989)
5. V.J. Emery, S. Kivelson, and O. Zachar, Phys. Rev. B **56**, 6120 (1997) and references therein.
6. L.P. Gorkov, A.V. Sokol, Pisma ZhETF, **46**, 333 (1987).
7. L.P. Gorkov, J. Supercond., **14**, 365, (2001).
8. U. Löw, V.J. Emery, K. Fabricious, and S. Kivelson Phys. Rev. Lett. **72** 1918 (1994).
9. F.V. Kusmartsev, Phys. Rev. Lett., **84**, 530, (2000), *ibid* **84**, 5026 (2000).
10. A.S. Alexandrov, V.V. Kabanov Pisma ZhETF, **72**, 825 (2000) (JETP letters, **72**, 569 (2000)).
11. F.V. Kusmartsev, J. Phys. IV, **9**, 321 (1999).
12. D.I. Khomskii, K.I. Kugel, Europhys. Lett. **55**, 208 (2001); Phys. Rev. B, **67**, 134401 (2003).

13. M.B. Eremin, A.Yu. Zavidonov, B.I. Kochelaev, ZhETF, **90**, 537 (1986).
14. S.R. Shenoy, T. Lookman, A. Saxena, A.R. Bishop, Phys. Rev. B, **60**, R12537 (1999); T. Lookman, S.R. Shenoy, K.O. Rasmussen, A. Saxena, and A.R. Bishop, Phys. Rev. B, **67**, 024114 (2003).
15. C. Ortix, J. Lorenzana, and C. Di Castro, Phys. Rev. B, **73**, 245117 (2006) and referece therein.
16. R. Jamei, S. Kivelson, and B. Spivak, Phys. Rev. Lett., **94**, 056805 (2005).
17. T. Mertelj, V.V. Kabanov, and D. Mihailovic, Phys. Rev. Lett. **94**, 147003 (2005)
18. T. Holstein, Ann. Phys.(N.Y.)**8**, 325, (1959); **8**, 343, (1959).
19. E.I. Rashba, Opt. Spektrosk. **2**, 78, (1957); **2**, 88, (1957)
20. V.V. Kabanov, O.Yu. Mashtakov, Phys. Rev. B, **47**, 6060, (1993).
21. A.S. Alexandrov V.V. Kabanov, D.K. Ray, Phys. rev. B **49**, 9915 (1994).
22. S.I. Pekar Zh. Eksp. Teor. Fiz. **16**, 335 (1946).
23. A.S. Alexandrov N.F. Mott Rep. Progr. Phys. **57**, 1197, (1994); *Polarons and Bipolarons* (World Scientific, Singapore, 1995).
24. S. Aubry, in: 'Polarons and Bipolarons in High- T_c Superconductors and Related Materials', eds E.K.H. Salje, A.S. Alexandrov and W.Y. Liang, Cambridge University Press, Cambridge, 271 (1995).
25. A.R. Bishop and M. Salkola , in: 'Polarons and Bipolarons in High- T_c Superconductors and Related Materials', eds E.K.H. Salje, A.S. Alexandrov and W.Y. Liang, Cambridge University Press, Cambridge, 353 (1995).
26. H. Fehske *et al*, Phys. Rev. **B51**, 16582 (1995).
27. J. Bonca *et al*, Phys. Rev. Lett., **84**, (2000).
28. A. Bianconi, J. Phys. IV France, **9**, 325 (1999) and references therein.
29. D. Mihailovic, V.V. Kabanov, Phys. Rev., B, **63**, 054505, (2001); V.V. Kabanov, D. Mihailovic, Phys. Rev., B, **65**, 212508, (2002).
30. A.R. Bishop, T. Lookman, A. Saxena, S.R. Shenoy, Europhys. Lett., **63**, 289, (2003).
31. J. Lajzerovicz, J. Sivardiere, Phys. Rev. **A11**, 2079 (1975).
32. J. Sivardiere, J. Lajzerovicz, Phys. Rev. **A11**, 2090 (1975)
33. N. Metropolis, A.W. Rosenbluth, M.N. Rosenbluth. A.H. Teller and E. Teller, *J. Chem. Phys.* **21**, 1087 (1953).
34. S. Kirkpatrick, C.D. Gelatt and M.P. Vecchi, Science 220 (1983) 671-680.
35. E.M.Lifshitz and L.P.Pitaevski, Physical Kinetics, ch.12 (Butterworth-Heinemann, 1980).
36. D.Reagor et al., Phys.Rev.Lett. **62**, 2048 (1989).
37. E.Dagotto, T.Hotta and A.Moreo, Phys. Rep. **344**, 1 (2001).; A.S. Alexandrov, A.M. Bratkovsky, and V.V. Kabanov, Phys. Rev. Lett., **96**, 117003 (2006).